

Long-term stability of capped and buffered palladium-nickel thin films and nanostructures for plasmonic hydrogen sensing applications

Nikolai Strohfeldt,* Andreas Tittl, and Harald Giessen

4th Physics Institute and Research Center SCoPE, University of Stuttgart, Pfaffenwaldring 57, D-70569 Stuttgart, Germany

*n.strohfeldt@physik.uni-stuttgart.de

Abstract: One of the main challenges in optical hydrogen sensing is the stability of the sensor material. We found and studied an optimized material combination for fast and reliable optical palladium-based hydrogen sensing devices. It consists of a palladium-nickel alloy that is buffered by calcium fluoride and capped with a very thin layer of platinum. Our system shows response times below 10 s and almost no short-term aging effects. Furthermore, we successfully incorporated this optimized material system into plasmonic nanostructures, laying the foundation for a stable and sensitive hydrogen detector.

©2013 Optical Society of America

OCIS codes: (160.3918) Metamaterials; (250.5403) Plasmonics; (280.4788) Optical sensing and sensors; (310.6845) Thin film devices and applications.

References and links

1. G. Marbán and T. Valdés-Solis, "Towards the hydrogen economy?" *Int. J. Hydrogen Energy* **32**(12), 1625–1637 (2007).
2. W. J. Buttner, M. B. Post, R. Burgess, and C. Rivkin, "An overview of hydrogen safety sensors and requirements," *Int. J. Hydrogen Energy* **36**(3), 2462–2470 (2011).
3. T. Hübert, L. Boon-Brett, G. Black, and U. Banach, "Hydrogen sensors - A review," *Sens. Actuators B Chem.* **157**(2), 329–352 (2011).
4. D. Nau, A. Seidel, R. B. Orzekowsky, S.-H. Lee, S. Deb, and H. Giessen, "Hydrogen sensor based on metallic photonic crystal slabs," *Opt. Lett.* **35**(18), 3150–3152 (2010).
5. E. M. Larsson, S. Syrenova, and C. Langhammer, "Nanoplasmonic sensing for nanomaterials science," *Nanophotonics* **1**(3–4), 249–266 (2012).
6. P. Albers, J. Pietsch, and S. F. Parker, "Poisoning and deactivation of palladium catalysts," *J. Mol. Catal. Chem.* **173**(1-2), 275–286 (2001).
7. S. Cataldo, J. Zhao, F. Neubrech, B. Frank, C. Zhang, P. V. Braun, and H. Giessen, "Hole-mask colloidal nanolithography for large-area low-cost metamaterials and antenna-assisted surface-enhanced infrared absorption substrates," *ACS Nano* **6**(1), 979–985 (2012).
8. P. Patnaik, *A Comprehensive Guide to the Hazardous Properties of Chemical Substances*, 3rd ed. (John Wiley & Sons, 2007), p. 1059.
9. F. A. Lewis, *The Palladium Hydrogen System*, 1st ed. (Academic Press Inc., 1967), p. 178.
10. M. Khanuja, B. R. Mehta, P. Agar, P. K. Kulriya, and D. K. Avasthi, "Hydrogen induced lattice expansion and crystallinity degradation in palladium nanoparticles: Effect of hydrogen concentration, pressure, and temperature," *J. Appl. Phys.* **106**(9), 093515 (2009).
11. P. Graviil and H. Toulhoat, "Hydrogen, sulphur and chlorine coadsorption on Pd(111): a theoretical study of poisoning and promotion," *Surf. Sci.* **430**(1-3), 176–191 (1999).
12. L. L. Sheu, Z. Karpinski, and W. M. H. Sachtler, "Effects of palladium particle size and palladium silicide formation on Fourier transform infrared spectra and carbon monoxide adsorbed on palladium/silicon dioxide catalysts," *J. Phys. Chem.* **93**(12), 4890–4894 (1989).
13. C. Langhammer, I. Zorić, B. Kasemo, and B. M. Clemens, "Hydrogen storage in Pd nanodisks characterized with a novel nanoplasmonic sensing scheme," *Nano Lett.* **7**(10), 3122–3127 (2007).
14. S. Wilke and M. Scheffler, "Poisoning of Pd(100) for the dissociation of H₂: a theoretical study of co-adsorption of hydrogen and sulphur," *Surf. Sci.* **329**(1-2), L605–L610 (1995).
15. J. Oudar, *Deactivation and Poisoning of Catalysts* (Taylor & Francis, 1985), p. 344.
16. P. Fedtke, M. Wienecke, M. Bunesco, M. Pietrzak, K. Deistung, and E. Borchardt, "Hydrogen sensor based on optical and electrical switching," *Sens. Actuators B Chem.* **100**(1-2), 151–157 (2004).
17. D. Stauffer and A. Aharony, *Introduction to Percolation Theory*, 2nd rev. ed. (Taylor & Francis, 1994), p. 192.

18. Z. Zhao, Y. Sevryugina, M. A. Carpenter, D. Welch, and H. Xia, "All-optical hydrogen-sensing materials based on tailored palladium alloy thin films," *Anal. Chem.* **76**(21), 6321–6326 (2004).
19. B. Chadwick, J. Tann, M. Brungs, and M. Gal, "A hydrogen sensor based on the optical generation of surface plasmons in a palladium alloy," *Sens. Actuators B Chem.* **17**(3), 215–220 (1994).
20. R. C. Hughes and W. K. Schubert, "Thin films of Pd/Ni alloys for detection of high hydrogen concentrations," *J. Appl. Phys.* **71**(1), 542–544 (1992).
21. R. C. Hughes, "Solid-state hydrogen sensors using palladium-nickel alloys: effect of alloy composition on sensor response," *J. Electrochem. Soc.* **142**(1), 249–254 (1995).
22. A. A. Yanik, M. Huang, O. Kamohara, A. Artar, T. W. Geisbert, J. H. Connor, and H. Altug, "An optofluidic nanoplasmonic biosensor for direct detection of live viruses from biological media," *Nano Lett.* **10**(12), 4962–4969 (2010).
23. A. E. Cetin and H. Altug, "Fano resonant ring/disk plasmonic nanocavities on conducting substrates for advanced biosensing," *ACS Nano* **6**(11), 9989–9995 (2012).
24. S. L. Teo, V. K. Lin, R. Marty, N. Large, E. A. Llado, A. Arbouet, C. Girard, J. Aizpurua, S. Tripathy, and A. Mlayah, "Gold nanoring trimers: a versatile structure for infrared sensing," *Opt. Express* **18**(21), 22271–22282 (2010).
25. N. Liu, M. L. Tang, M. Hentschel, H. Giessen, and A. P. Alivisatos, "Nanoantenna-enhanced gas sensing in a single tailored nanofocus," *Nat. Mater.* **10**(8), 631–636 (2011).
26. C. Langhammer, E. M. Larsson, B. Kasemo, and I. Zorić, "Indirect nanoplasmonic sensing: ultrasensitive experimental platform for nanomaterials science and optical nanocalorimetry," *Nano Lett.* **10**(9), 3529–3538 (2010).
27. T. Shegai, P. Johansson, C. Langhammer, and M. Käll, "Directional scattering and hydrogen sensing by bimetallic Pd-Au nanoantennas," *Nano Lett.* **12**(5), 2464–2469 (2012).
28. K. M. Mayer and J. H. Hafner, "Localized surface plasmon resonance sensors," *Chem. Rev.* **111**(6), 3828–3857 (2011).
29. M. A. Poyli, V. M. Silkin, I. P. Chernov, P. M. Echenique, R. D. Muiño, and J. Aizpurua, "Multiscale theoretical modeling of plasmonic sensing of hydrogen uptake in palladium nanodisks," *J. Phys. Chem. Lett.* **3**(18), 2556–2561 (2012).
30. T. Weiss, N. A. Gippius, S. G. Tikhodeev, G. Granet, and H. Giessen, "Derivation of plasmonic resonances in the Fourier modal method with adaptive spatial resolution and matched coordinates," *J. Opt. Soc. Am. A* **28**(2), 238–244 (2011).
31. T. Weiss, N. A. Gippius, S. G. Tikhodeev, G. Granet, and H. Giessen, "Efficient calculation of the optical properties of stacked metamaterials with a Fourier modal method," *J. Opt. A, Pure Appl. Opt.* **11**(11), 114019 (2009).
32. W. Vargas, I. Rojas, D. Azofeifa, and N. Clark, "Optical and electrical properties of hydrided palladium thin films studied by an inversion approach from transmittance measurements," *Thin Solid Films* **496**(2), 189–196 (2006).
33. A. B. Dahlin, J. O. Tegenfeldt, and F. Höök, "Improving the instrumental resolution of sensors based on localized surface plasmon resonance," *Anal. Chem.* **78**(13), 4416–4423 (2006).

1. Introduction

In recent years, advances in fuel cell based transportation and energy storage have stimulated immense growth in material science and industry. In this emergent hydrogen economy [1], the reliable and sensitive detection of hydrogen is crucial to ensure the safety of industrial workers and consumers alike [2].

One possible solution to fulfill these requirements is an optical hydrogen sensor based on plasmonic palladium nanostructures [3–5]. The optical excitation and readout minimizes the risk of self-ignition, while the plasmonic palladium structures provide a highly sensitive and hydrogen-specific detection method.

In this work, we investigate one of the main challenges in palladium-based hydrogen sensing systems, namely the long-term stability, the aging, and performance degradation caused by the prolonged use with hydrogen and exposure to pollutants in the atmosphere [6]. We first focus on thin films of palladium and palladium-based materials to optimize the hydrogen sensing performance. We then incorporate these materials into nanostructured plasmonic sensing geometries, laying the foundation for reliable and long-term stable nanosensors.

2. Measurement setup

In order to investigate our thin-film samples, we use a homebuilt optical sensor device (Fig. 1). It consists of an ultra-bright red Light Emitting Diode (LED, center wavelength 630 nm) and two photo-diodes (PD1, PD2) measuring the reflected and the transmitted light from the

sample. We use SiO₂ substrates (7.5 x 7.5 x 1 mm) with hydrogen sensitive films evaporated on top. The sample is fixed in a polyoxymethylene (POM) casing and protected from stray-light via a gas-permeable sinter metal cylinder. These components, together with the read-out electronics are housed in a robust and compact stainless steel sensor head. Small holes at the sides of the cylindrical sensor head allow for unimpeded flow of the gas mixture, yielding reliable and reproducible measurements.

To obtain stable signals, the output needs to be independent of the LED's light intensity. Otherwise, aging-induced degradation of the diode as well as fluctuations in the power supply could influence the signal.

This is realized by a feedback loop that adjusts the LED's voltage to keep the current of photo diode 1 (PD1) and therefore the reflection signal R constant ($R = I_0 \cdot r = const.$). Hence, the output signal S , which is proportional to the current of photo diode 2 (PD2) and therefore proportional to the transmitted light $T = I_0 \cdot t$ can be written in terms of only the transmittance t and reflectance r :

$$S \propto T \propto \frac{t}{r}$$

This output signal S is closely related to the optical properties of the thin film sample and can therefore be used to monitor changes in its dielectric function due to hydrogen exposure.

One big advantage of our setup is that we are not restricted to measurements on simple thin film geometries. Consequently, our system can be used to investigate a multitude of large-area structures that change their extinction/transmission spectrum under the influence of gaseous reagents. It can, e.g., easily be transferred to large-area plasmonic structures [7] with much higher sensitivity.

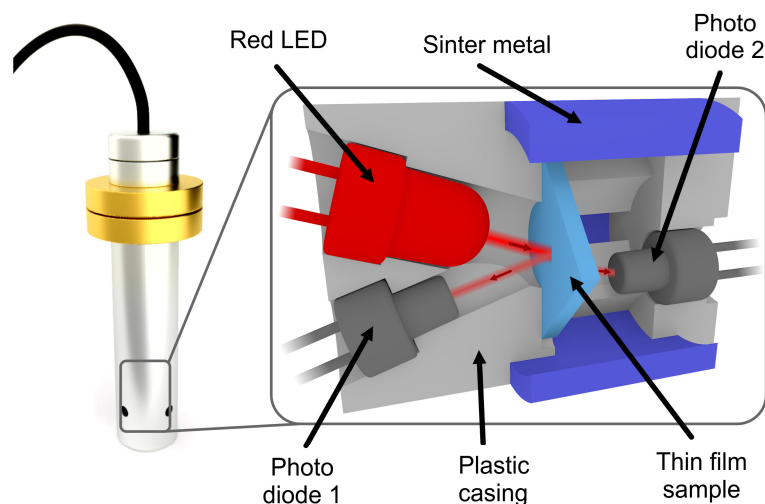


Fig. 1. (Left) Overview of the complete sensor device. (Right) Schematic drawing of the H₂-sensor head used to measure the reflected and transmitted light from our thin film samples. The sample is surrounded by a sinter metal cylinder which permits hydrogen diffusion but blocks stray light. Illumination is done by a red LED with a center wavelength of 630 nm.

To obtain accurate gas dependent measurements, the sensor is connected via stainless steel gas tubes to a custom-built gas mixing system consisting of several Bronkhorst mass flow controllers that allows us to precisely adjust and monitor the flow rates of several gases at once. In our measurements, we use various amounts of high-purity hydrogen in nitrogen as a

carrier gas. This results in an easy to handle environment and avoids combustible hydrogen-oxygen mixtures.

The lower explosion limit of hydrogen in air is 4 vol.% [8]. Hence, a possible sensing device has to show pronounced reactions to hydrogen concentrations well below this limit. Therefore, we use gas cycles of 0.5 - 3 vol.% H₂ in N₂ to characterize our samples. Between concentration steps, the samples are flushed with pure N₂ to check the reproducibility of the hydrogen loading/unloading process. All gas measurements are carried out at room temperature, with a constant gas flow of 1 l_n/min.

3. Thin film measurements

3.1 Pure palladium samples

Figure 2(a) shows the reaction of a 20 nm pure palladium film to hydrogen exposure. A typical hydrogen-nitrogen cycle consists 0.5, 1, 2 and 3 vol.% H₂ in N₂, with pure N₂ flushing steps in between subsequent H₂ concentrations (Fig. 2(d)).

We use time-steps of 200 s for all the samples. This allows the system to reach equilibrium after each concentration change. Furthermore, we always record at least three consecutive exposure cycles to ensure consistency between measurements.

Figure 2(a) shows the sensor signal of a freshly evaporated palladium film without previous exposure to hydrogen (black line). We can observe a pronounced reaction to the different hydrogen concentrations and response times well below 50 s for 1 and 2 vol.% H₂. For concentrations of 2 and 3 vol.% H₂, the reaction time as well as the amplitude noticeably increases.

This nonlinear behavior of the palladium can be attributed to a phase change that is accompanied by structural changes [9]. For low concentrations (α -phase), hydrogen ions only occupy the interstitial sites of the fcc Pd-lattice without significantly changing the lattice structure. When the hydrogen concentration is increased, the palladium-hydride (the β -phase) forms and causes a significant lattice expansion [10]. This phase change behavior also explains the increased response time, since the restructuring adds an additional time factor to the otherwise diffusion-governed process.

When measuring the same sample again 4 and 11 days after the first exposure, a strong degradation of the signal amplitude and especially the response time is visible (Fig. 2(a)). After 4 days, the signal amplitude is already cut in half and the response time more than triples (more detailed discussion below).

Literature and our experiments show that there are two main reasons for this behavior, namely external atmospheric influences that damage the palladium film [6,11,12] as well as internal changes of the palladium lattice itself that are triggered by the hydrogen exposure [9,13].

Comparisons between aged films with and without prior hydrogen exposure show that samples without a hydrogen history still show some degeneration (black solid and dotted lines in Fig. 2(a)). This proves that the film is changed by the hydrogen itself (comparing the black dotted and the red line in Fig. 2(a)) and also by other external factors such as atmospheric gases that interact with the sensor (comparing the solid and dotted black line).

It is known from literature that palladium surfaces can be (partially) deactivated by poisoning with sulfur, methane, or other atmospheric gases [6,11,14,15]. This necessitates a protective layer to prevent surface contamination.

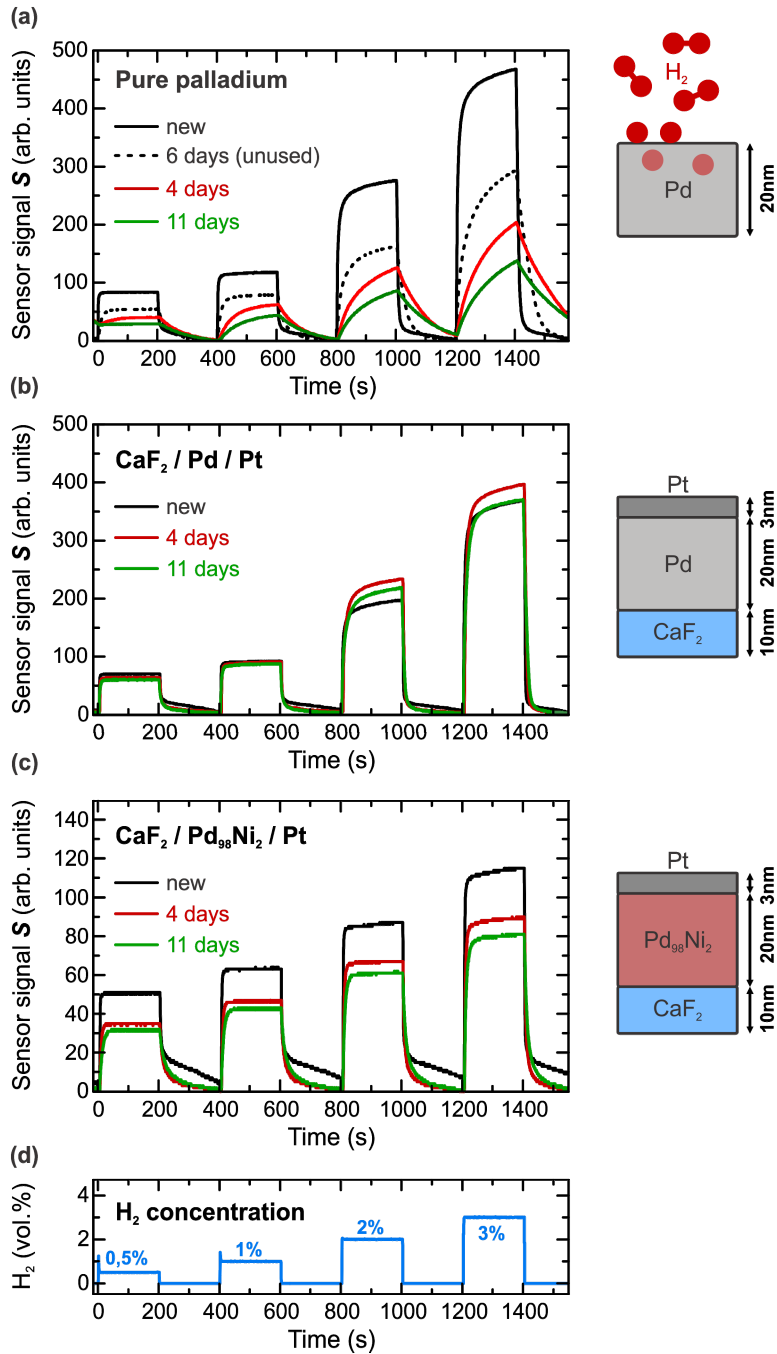


Fig. 2. (a) Sensor signal S of a 20 nm pure palladium thin film sample exposed to different concentrations of hydrogen. Measurements were performed for freshly evaporated, 4 days and 11 days old samples, as well as for a 6 days old sample without prior hydrogen exposure. (b) Improved sensor geometry consisting of a 20 nm Pd thin film buffered by 10 nm CaF₂ and capped by 3 nm Pt, minimizing sample degradation. (c) Sensor response of a capped and buffered Pd-Ni alloy sample (Pd₈₈Ni₂), showing improved response times and linearity. All measurements were performed under identical experimental conditions using the gas cycle displayed in (d).

The internal changes in the Pd, namely in lattice constant and size of the palladium film during hydrogen cycling also influence its substrate-adhesion and, over time, can lead to blistering and cracking of the film. There are two approaches for preventing this problem. First, palladium can be alloyed with different metals in order to reduce the effects of the lattice expansion. Second, a buffering or mediating layer can be introduced to improve the adhesion between palladium and the substrate. Both approaches can lead to reduced stress in the palladium and therefore make the system more stable.

3.2 Optimized material system

Fedtke et al. propose the use of a thin layer of calcium fluoride (CaF_2) to improve the surface adhesion of palladium. Additionally, they recommend a capping layer of platinum to reduce atmospheric poisoning [16]. To test this approach, we use 10 nm CaF_2 (to ensure a continuous film) below a 20 nm palladium film, evaporated in a single vacuum process. As capping layer we evaporate 3 nm platinum. The thickness of the platinum is well below the percolation threshold [17] and therefore, hydrogen diffusion into the palladium is not hindered. This thin layer does not cover the Pd completely, but was found to be the best compromise between surface protection and response time. In addition, the catalytic nature and high surface area of the granular platinum islands can aid the splitting of H_2 into atomic hydrogen.

Figure 2(b) shows the reaction of the capped and buffered palladium sample to a standard hydrogen cycle. The reactions of freshly evaporated films (black curves in Figs. 2(a) and 2(b)) are almost identical. Only the amplitude of the signal is slightly lower for the capped and buffered geometry. However, this is easily explained by the additional platinum layer that lowers the output signal S .

Compared to the strong changes in the aging Pd, the 4 and 11 days old CaF_2 / PdNi / Pt samples show almost no visible degradation effects. In the response times and amplitudes only slight changes are visible. For 2 and 3 vol.% hydrogen exposure, the signal for the 4 and 11 days old sample exceeds the one for the new sample and shows a faster relaxation. This can be understood best in a microscopic picture. When the hydrogen is incorporated into the Pd-lattice, the lattice expansions and compressions lead to a stress-reducing restructuring of the film. Only after this “training”-period is completed, the signal becomes stable.

We now address the non-linear sensor response in pure palladium systems. This non-linearity can be associated with the onset of the transition between α - and β -phase. One possibility to suppress, or at least shift this phase change to higher hydrogen concentrations, is to alloy palladium with other metals like gold [18] or nickel [19,20]. By alloying it with only small amounts of nickel a substantial shift of the transition pressure can be achieved [21].

Figure 2(c) shows the reaction of a $\text{Pd}_{98}\text{Ni}_2$ film (2 at.% nickel), capped and buffered with platinum and calcium-fluoride. This film was prepared, using commercially available PdNi pellets containing 5 at.% nickel. However, due to different vapour pressures of Pd and Ni, the true nickel content of the film (as determined by XPS measurements) is only about 2 at.%.

The nickel successfully shifts the transition pressure above 5 vol% H_2 , leading to a linear signal/concentration ratio. This happens at the expense of signal strength, leaving only a quarter of the original amplitude at 3 vol.% H_2 . However, the reduced signal leads to an improved response time, which is even smaller than for the capped and buffered Pd in Fig. 2(b). In addition, the response times stay nearly constant over time.

To further investigate the linearity of the signal and also the influences of the capping and buffering, Fig. 3 shows a comparison of the equilibrium amplitudes for hydrogen concentrations between 0.5 and 5 vol.% hydrogen. All amplitudes are normalized to a sensor signal S of pure Pd at 0.5 vol.% H_2 . The data shows that capping and buffering only has negligible influence on the amplitudes of the sensor signal.

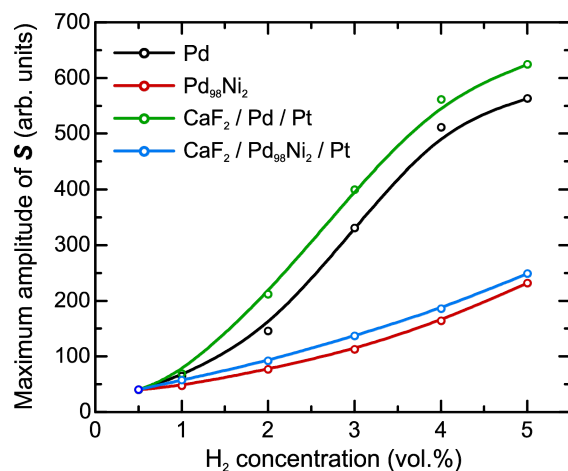


Fig. 3. Maximum amplitude of the sensor signal S for different aged thin film material systems at H_2 concentrations ranging from 0.5 to 5 vol.% H_2 in N_2 . For the $Pd_{98}Ni_2$ layers both with and without capping and buffering, we observe a nearly linear response whereas the non-alloyed Pd samples exhibit logistic like behavior. However, utilizing palladium-nickel alloys in place of pure Pd reduces the maximum sensor response S .

This means that the capping and buffering layers do not influence the film's ability to incorporate hydrogen. Only alloying the palladium strongly changes the amplitudes by shifting the phase transition.

Not only the amplitudes but also the response times can be very different for the different materials. Figure 4 shows an overview of all the response times for the capped, buffered, or alloyed samples. To characterize the samples we define the rise time TR8 to be the time until 80% of the maximal amplitude is reached and the fall time TF8 until 80% of the baseline signal is restored. Figure 4 shows the rise and fall time of a 4 days old $CaF_2 / Pd_{98}Ni_2 / Pt$ sample exposed to 2 vol.% H_2 .

The rising time TR8 is on the order of 5 s, and after 15 s the maximum signal is reached (Fig. 4(a)). When comparing the blue dotted curve (H_2 concentration) to the red one (sensor signal), there is a small discrepancy at the beginning (marked TG), attributed to the traveling time of the gas mixture from the mass flow system to the sensor head. In all measured material systems, TG is approximately 3 seconds, independent of material, age, or H_2 concentration.

We now compare the rising and falling times TR8 and TF8 of the different material systems at different ages. The insets in Figs. 4(a) and 4(b) show TR8 and TF8 for 2 vol.% H_2 . The insets in Fig. 4 show that the response times for the non-buffered and non-capped Pd/PdNi samples quickly exceed one minute while aging. This disqualifies them for sensor applications.

All other samples already exhibit response times below one minute. However, only the capped and buffered PdNi system (magenta line) delivers rise times TR8 below 10 s, making it suitable for industrial applications.

Although the fall times TF8 of the non-alloyed, capped, and buffered sample are slightly superior, the PdNi sample still shows a fast response with TF8 below 30 s.

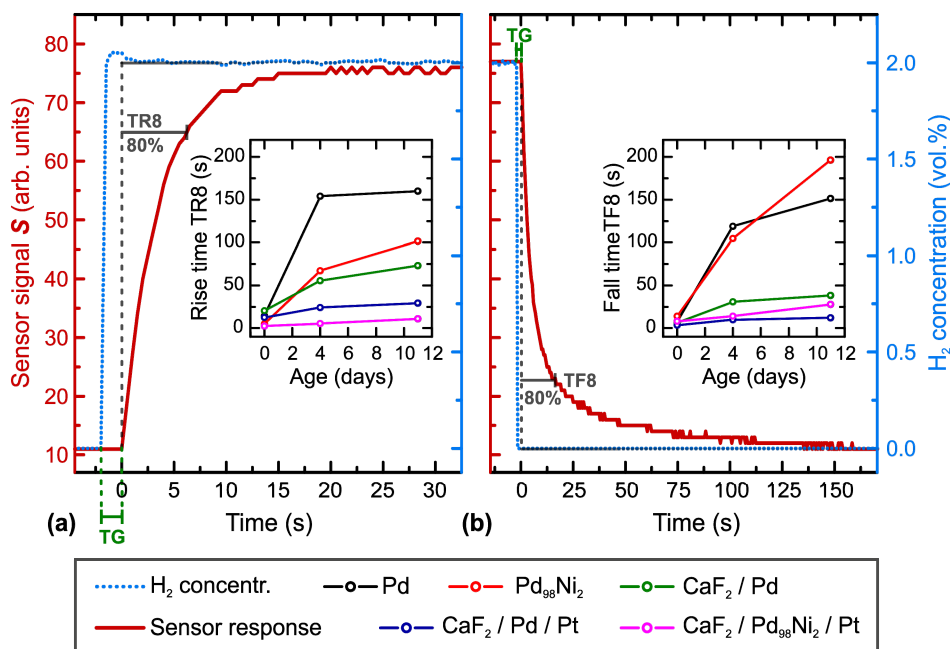


Fig. 4. (a) Response time TR8 of the H₂ sensor for a 4 days old CaF₂ / Pd₉₈Ni₂ / Pt sample exposed to 2 vol.% hydrogen. TG is the time till the gas reaches the sample volume and TR8 is the time until 80% of the maximum sensor signal S is reached. The inset shows response times for different material systems at different ages. (b) The relaxation time of the CaF₂ / Pd₉₈Ni₂ / Pt sample. TF8 is the time when 80% of the initial state (0% H₂ in N₂) is restored. The inset again shows the comparison with the other material systems. In both cases, the optimized material system (CaF₂ / Pd₉₈Ni₂ / Pt) shows greatly reduced time constants TR8 and TF8 compared to pure Pd and Pd₉₈Ni₂ films.

4. Nanoparticle measurements

We proceed to incorporate our improved material system into more sophisticated plasmonic sensor structures. Plasmonic resonances in metal nanoparticles can have a tremendous impact on the performance of sensing devices [22–24], especially hydrogen sensors [25–27].

Localized surface plasmon resonances (LSPRs) in metal nanoparticles are coherent oscillations of the conducting electrons that are highly dependent on the dielectric function of the metal and its surroundings as well as on the shape and size of the structures [28].

Palladium shows a plasmonic resonance in the visible or near infrared spectral region [13]. This resonance exhibits a pronounced redshift upon hydrogen exposure, due to dielectric changes in the Pd [29].

As a model system for the investigation of nanostructured hydrogen sensors and their aging behavior, we choose simple palladium nanodisks.

We first perform numerical simulations to find suitable disk-dimensions that yield plasmon resonances in the wavelength region of interest (500 to 1000 nm). These simulations were performed using a scattering matrix approach [30,31] with the dielectric functions for Pd and PdH taken from literature [32].

The numerical calculations show that disks with a diameter of 200 nm and a height of 20 nm exhibit a plasmon resonance for both Pd and PdH in the selected wavelength range (Pd resonance at 744 nm and PdH resonance at 964 nm). We choose a disk height of 20 nm to facilitate the comparison between thin film and nanoparticle experiments.

Two different samples with palladium nanodisk arrays (periodicity 900 nm) were fabricated via electron-beam lithography: one with Pd disks buffered with 10 nm CaF₂ and capped with 3 nm Pt and the other with pure Pd disks on a SiO₂ substrate. We only used capped and buffered Pd nanodisks because the plasmonic behavior of palladium is well established in literature, whereas the plasmonic properties of PdNi have not yet been investigated theoretically or experimentally.

Figure 5(a) shows transmission spectra of the capped and buffered disk arrays for different hydrogen concentrations. These spectra were measured under bright-field illumination conditions using an inverted microscope combined with a spectrometer with attached CCD camera. We observe a clear redshift and broadening of the plasmon resonance that increases with higher concentrations of hydrogen. This behavior is in very good agreement with the numerical simulations and can be fully explained by changes in the dielectric function of the material.

In addition, we perform time-resolved transmission measurements while changing the hydrogen concentration from 0 to 3 vol.% in the same time-steps as for the thin film measurements. We record spectra every 8 s with an integration time of 5 s per spectrum. In order to track the spectral position of the LSPR, we compute the centroid wavelength from the spectral data. The centroid method is a way to accurately extract even small spectral shifts from noisy data by tracking the “center of mass” of a spectral feature [33].

In Figs. 5(b)-5(e) centroid time traces of both pure and capped/buffered Pd disk arrays are shown. The pure Pd disks exhibit the expected strong reaction to hydrogen exposure with a centroid shift of 65 nm for 3 vol.% H₂ (Fig. 5(b)). However, if one compares the reactions to 2 and 3% H₂, both have almost exactly the same centroid wavelength after they reach equilibrium. This and the large jump between 1 and 2 vol.% H₂ indicates that the transition between α - and β -phase happens already below a level of 2 vol.% hydrogen. Contrarily, in thin film measurements we only observe such a flattening of the sensor response for hydrogen concentrations around 5 vol.%. This proves the known and accelerated phase change in palladium nanoparticles [13].

Figure 5(c) displays the centroid time trace of the same Pd-disk array 2 days after the first exposure. Similar aging and degeneration signs are visible as for the thin films: strong increase in the response time and decrease of the signal amplitude or in this case of the resonance redshift. The biggest difference between the aging behavior of the disks and thin films is the pace at which the degeneration process is happening. The increase of the response times of the disks, happening in two days is already worse than one of a pure Pd film after more than a week. This effect might be explained by the strongly enhanced surface/volume ratio in the palladium disks that causes faster poisoning of the surface.

In contrast, the capped and buffered palladium disks (Figs. 5(d) and 5(e)) show a very different aging behavior. Almost no change in centroid-wavelength shift is visible for the new and two days old sample. Both the response times and wavelength shift stay constant. The slight blueshift of the centroid-wavelength can be attributed to the alignment of the measurement setup. Although the hydrogen induced sensor response is somewhat reduced (30 nm redshift compared to 65 nm in the pure Pd disks), it is still more than sufficient for practical applications. This reduction may be explained by formation of a PdPt alloy at the surface that lowers the solubility of hydrogen in the disk.

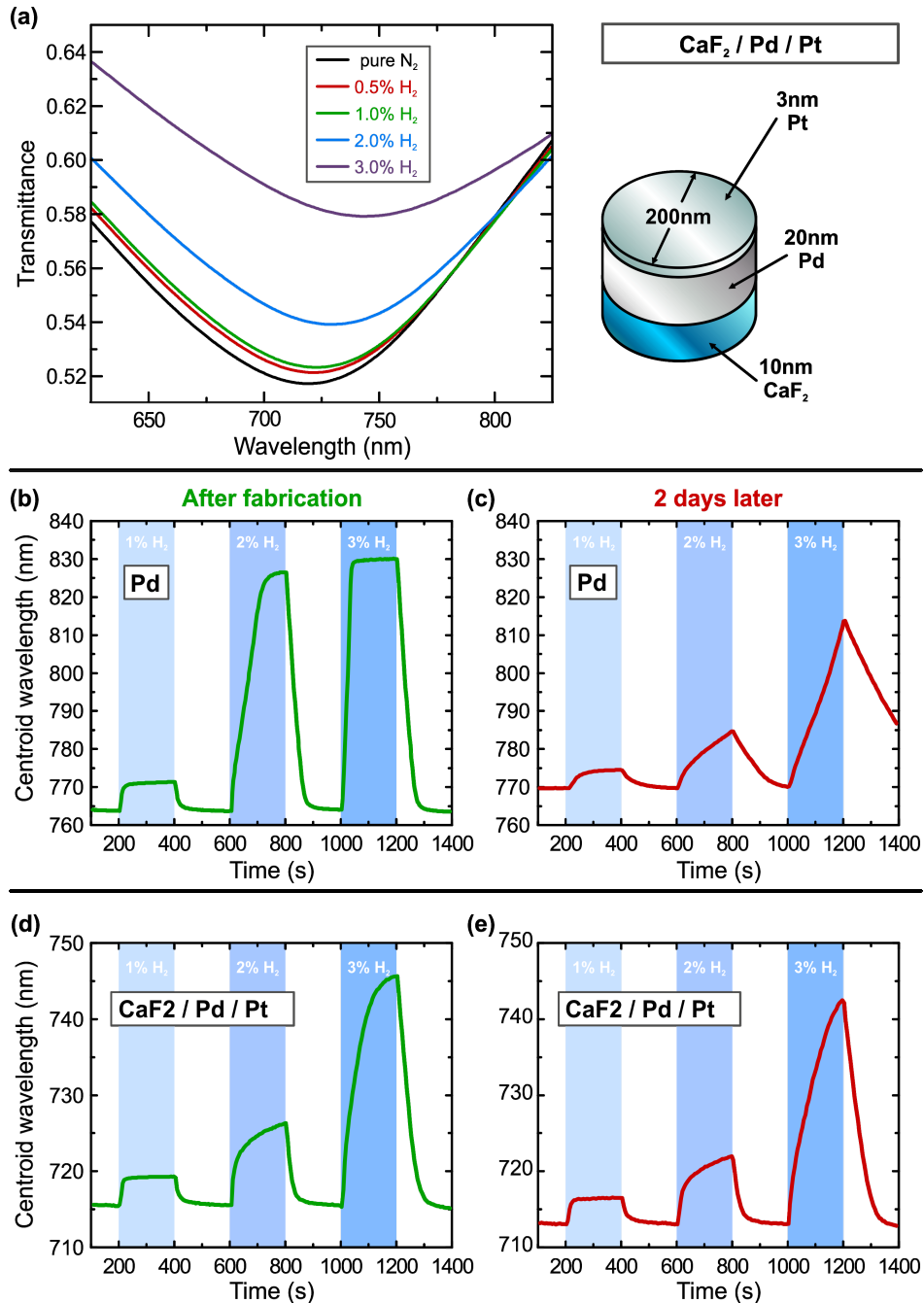


Fig. 5. (a) Transmission spectra of a $\text{CaF}_2 / \text{Pd} / \text{Pt}$ nanodisk array, exposed to cycles of 0.5 to 3.0 vol.% H_2 in N_2 , showing a redshift and broadening of the plasmon resonance. (b) Time-resolved dynamics of the plasmon centroid wavelength under hydrogen exposure, measured for a newly fabricated pure Pd nanodisk array sample. (c) Centroid wavelength trace of the same sample two days later, showing substantially increased response time and reduced redshift under hydrogen exposure. (d) Time-resolved dynamics of the plasmon centroid wavelength, measured at Pd disks capped with 3 nm Pt and buffered with 10 nm CaF_2 . (e) Centroid wavelength trace of the $\text{CaF}_2 / \text{Pd} / \text{Pt}$ sample. It was prepared, stored and measured under the same conditions as in (c) but shows almost no degradation.

5. Conclusion and outlook

We found and studied a material combination for optical hydrogen sensing that shows a very good temporal stability while still providing a strong signal in reaction to hydrogen exposure. This material system consists of a palladium-nickel alloy, a calcium fluoride buffer and a platinum capping layer. It was shown that the stress of the palladium film can be reduced by the calcium fluoride buffer. The surface poisoning is avoided by a platinum capping and the phase transition can be suppressed by alloying the palladium with nickel. The functionality of the material was proven in aging studies of different thin films. Although this study was conducted under ambient atmospheric conditions, without the controlled exposure to specific pollutants or hazardous gases, our experiments represent the first steps towards a fully stable and robust sensing material.

Furthermore, studies with palladium nanodisks show that it is possible to use the insights gained in thin films to improve the durability and stability of nanoparticle based sensors. Hence, our system is perfectly suitable for hydrogen sensors based on thin films as well as plasmonic nanoparticles.

Future work with more complex plasmonic sensing schemes will greatly benefit from this enhanced durability and therefore enable, for the first time, industrially viable plasmonic hydrogen sensing systems.

Acknowledgments

We acknowledge support by the DFG (SPP1391, FOR730, and GI 269/11-1) the BMBF (13N9049 and 13N10146) and the Baden-Württemberg Stiftung (Kompetenznetz Funktionelle Nanostrukturen). The authors would like to thank Jens Dorfmueller and Martin Schaferling for stimulating discussions as well as Claudia Kamella and Viola Duppel from the Max-Planck-Institute for Solid State Research, Stuttgart for performing the XPS measurements at the PdNi films. This work was supported by the German Research Foundation (DFG) within the funding program Open Access Publishing.